## DETC2022-93913

# CHARACTERIZATION OF NONLINEAR KIRIGAMI SPRINGS THROUGH TRANSIENT RESPONSE

#### Francesco Danzi\*

School of Mechanical Engineering and Ray W. Herrick Laboratories Purdue University West Lafayette, Indiana, 47907 Email: fdanzi@purdue.edu

## **Hongcheng Tao**

School of Mechanical Engineering and Ray W. Herrick Laboratories Purdue University West Lafayette, Indiana, 47907 Email: taoh@purdue.edu

## Joshua Jenkins

DMC Chicago, IL, 60614 Email: joshua.jenkins9816@gmail.com

#### James M. Gibert

School of Mechanical Engineering and Ray W. Herrick Laboratories Purdue University West Lafayette, Indiana, 47907 Email: jgibert@purdue.edu

#### **ABSTRACT**

Kirigami is defined as the ancient Japanese art of cutting and folding paper to create three-dimensional structures, which is a subset of the larger term. Recent developments in kirigamibased structures have sparked interest in the engineering community for the development of mechanical metastructures with customized behavior such as negative Poisson's ratio, out-of-plane buckling, and soft robot locomotion. In this manuscript, nonlinear springs based on kirigami are developed; the springs can be used to create customized nonlinear oscillators and vibration suppression systems. A Helmholtz-Duffing oscillator with nonlinear damping is created by attaching a mass to a smooth track with the kirigami springs attached to it.

Kirigami springs were made by strategically cutting plastic sheets in predetermined patterns and arranging them in a ring. Identification of the unknown system parameters is accomplished through the use of a two-step procedure. To determine the quasistatic behavior of the spring, it was first subjected to tensile testing. These parameters serve as the foundation for developing a strategy for determining the unknown energy loss parameters in a system. In the second step, the Method of Multiple Scales is used to develop an approximate solution for the transient response, which is then tested. This solution is coupled with an optimization routine that, by modifying the unknown model parameters, seeks to reduce the error between the experimental free oscillations and the developed analytical solution as closely as possible.

## 1 INTRODUCTION

Kirigami is the Japanese craft of paper cutting. It is a variation of origami that is based on 3-dimensional cutting of paper rather than folding. The word kirigami is derived from two Japanese words "kiri" meaning to cut and "kami" meaning paper. While the origami has been widely used to inspire the design of novel engineering structures and materials [1,2,3]. Kirigami has only recently been used to inspire the engineering community to application ranging from grasping robots [4], programmable

<sup>\*</sup>Address all correspondence to this author.

shapes [5], crawling robots [6], to morphable structures [7]. To the author's knowledge, the use of kirigami in vibration applications is largely unexplored and is currently with prominent example being studies characterizing the modal properties of kirigami structures [8], flexural wave control [9], and pressure sensing via a resonant circuit [10].

The purpose of this study is to characterize the properties of kirigami springs that are slitted membranes through the use of static and dynamic tests. The proposed springs provide a straightforward method for tuning the stiffness of a system and may be used to design novel nonlinear oscillators.

## 2 MOTIVATION

Assuming that the kirigami spring's resistive force can be decomposed into elastic and viscous components then the linear elastic behavior of the programmable kirigami springs is based on two concepts: geometric nonlinearity and topological modification of stiffness through various cutting patterns. The concept is best illustrated by considering a stretched membrane of length L. Using a one-dimensional approximation a kirigami spring that is stretched in its elastic region and subject to a static force F will experience a transverse displacement. The relationship between the force and displacement can be written as

$$F = k \left( 1 - \frac{L_o}{\sqrt{(\Delta L + L_o)^2 + x^2}} \right) x,\tag{1}$$

where k is the characteristic stiffness of the string and  $\Delta L$  is the stretch in the spring due to the application of the spring. Considering small displacements, the fractional term in Eqn. (1) can be written as

$$\frac{1}{\sqrt{(\Delta L + L_o)^2 + x^2}} \approx \frac{1}{\Delta L + L_o} - \frac{x^2}{2(\Delta L + L_o)^3} + \frac{3x^4}{8(\Delta L + L_o)^3} + \mathcal{O}(x^6), \tag{2}$$

using a Taylor series expansion about x = 0. The force displacement relationship can then be approximated as

$$F \approx k \left( \left( \frac{\Delta L}{\Delta L + L_o} \right) x + \left( \frac{L_o}{2(\Delta L + L_o)^3} \right) x^3 \right) + \mathcal{O}(x^5), \quad (3)$$

where  $k = EA/L_{eff}$ . Note that nominally  $L_{eff} = \Delta L + L_o$ . Examining Eqn. (3) reveals two paths to change the force displacement relationship given a fixed geometric configuration. The first is to change the stretch  $\Delta L$  in the spring and the second is to modify

the effective stiffness of the material. The concept introduced in this work is to modify k by having changes in  $L_{eff}$  through the introduction of cuts in the membrane.

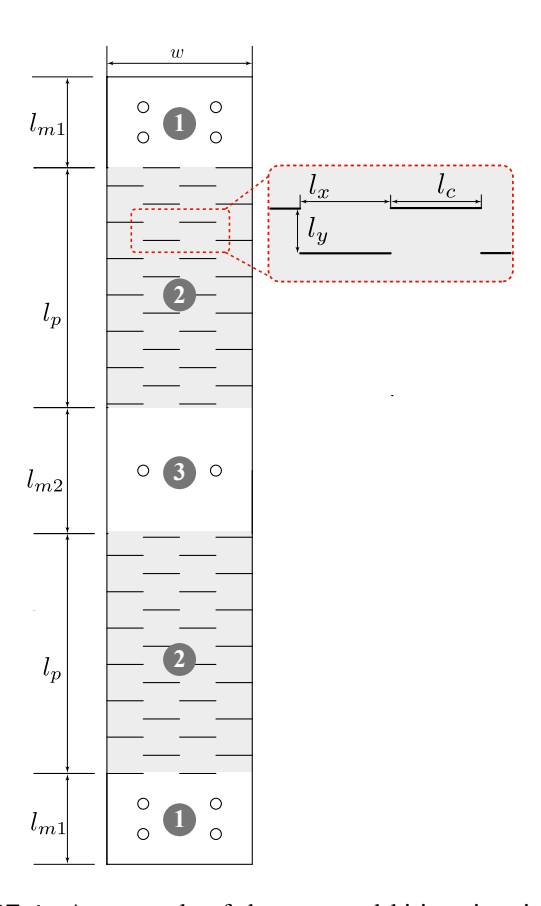


**FIGURE 1**: An example of the proposed kirigami spring with annotated segments and dimensions. Sections in grey indicate the programmable region. Inset shows the characteristics of each pattern. The specimens in this work have characteristics  $l_{m1} = 30.0 \text{ mm}$ ,  $l_{m2} = 40.0 \text{ mm}$ ,  $l_p = 80.0 \text{ mm}$ , and w = 48.0 mm.

## 3 MATERIALS AND METHODS

This section describes the manufacturing process for kirigami springs, as well as the static and dynamic tests used to characterize their properties. The springs are made of Grafix sheets that measure 304.8 mm by 304.8 mm and have a thickness of 0.1778 mm. A Silhouette Cameo cutter is used to cut 260 mm long by 48 mm wide sheet springs. The springs are made up of three segments: 1) a mounting segment of 30 mm to ground the spring, 2) an active section of 80 mm that is the *programmable region*, and 3) a 40 mm segment to attach the spring to a proof mass or directly apply a load. Sections 1) and 2) are mirrored

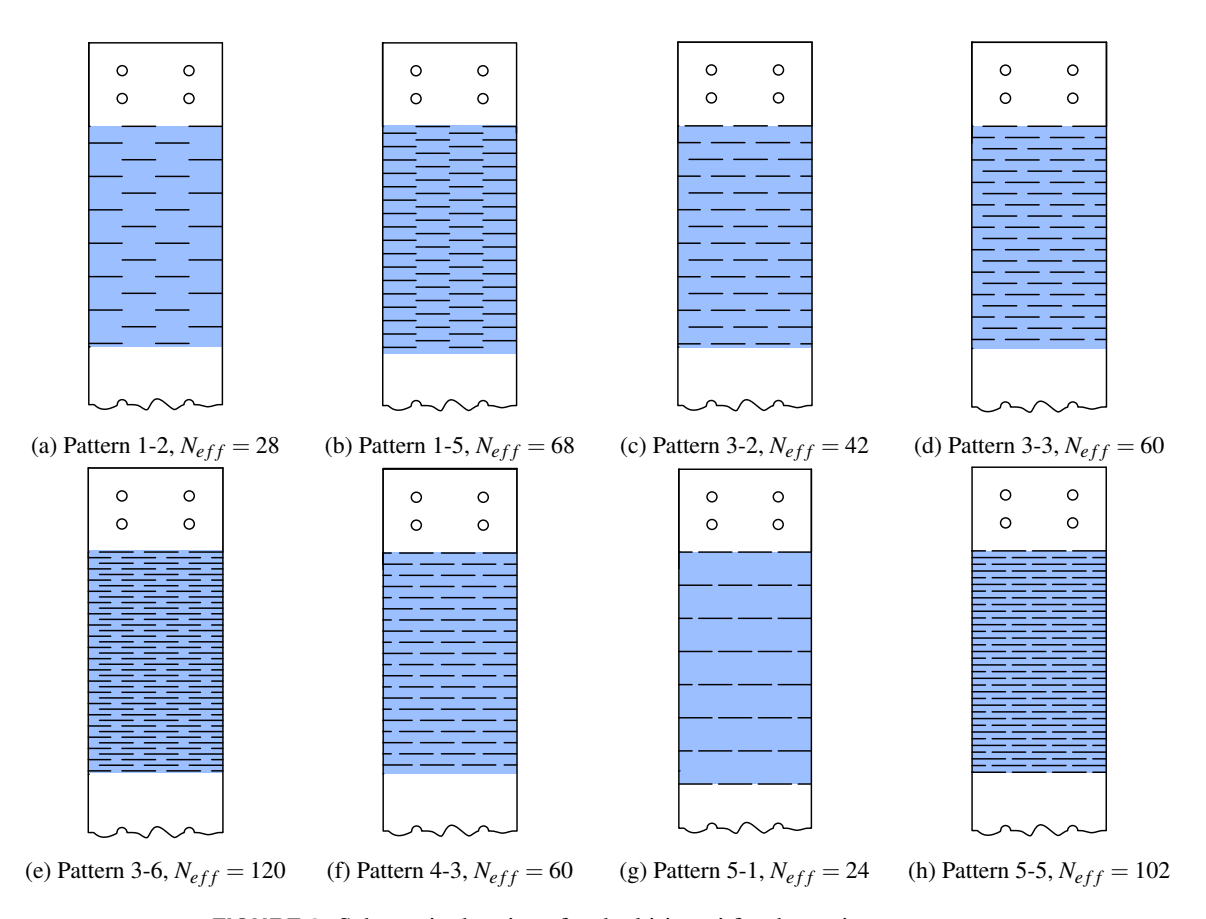


FIGURE 2: Schematic drawings for the kirigami for the various patterns.

about the center of the spring, Fig. 1. Segments 1) and 3) contain mounting holes to secure the spring to ground or a mass.

#### 4 Pattern Selection

In order to fully exploit the observations in previous section a characterization of the relationship between kirigami pattern and mechanical characteristics, a pattern of straight, horizontal cuts on a rectangular spring was chosen, Fig. 1. Eight samples were chosen and based on the work of Yang et al. [11], the length of cut is designated  $l_c$  and the horizontal spacing is  $l_x$ , while the vertical spacing  $l_v$ . For this work, a constant cut length ( $l_c$ ) of 12 mm was used such that only the spacing of cuts are varied between patterns. The patterns are designated as by the nomenclature  $l_c/l_v$  -  $l_c/l_x$ . Eight patterns are considered in this work patterns 1-2, 1-5, 3-2, 3-3, 3-6, 4-3, 5-1, and 5-5 where five specimens are created for each pattern. Finally, the number of effective cuts,  $N_{eff}$ , in the turning region is calculated; the number of complete cuts is counted; smaller counts are added and rounded to a complete cut. It should be noted that due to the loading of the springs the multistable behavior of the structures proposed by

Yang et al. [11] are not retained but their designation provides an efficient methodology to introduce patterns that will change the effective stiffness of the spring.

#### 5 Quasi-Static Testing

A Mark-10 ESM 1500 motorized tension test stand was used to perform quasi-static testing to determine the force displacement relationship of the springs due to the geometric nonlinearity. The springs are tested at rate of 50 mm/min. As shown in Figure 3b, the springs were mounted on 3D printed test stands that were positioned so that each spring was initially stretched by 5 mm before the Mark 10 was lowered to introduce additional tension to the spring. Each spring was subjected to a displacement that alternated between the initial configuration and a peak displacement of 30 mm using this setup. Each specimen was loaded a total of five times. A minimal amount of hysterisis was evident between the loading and unloading curve and the average of these curves was used for the quasi-static characterization.

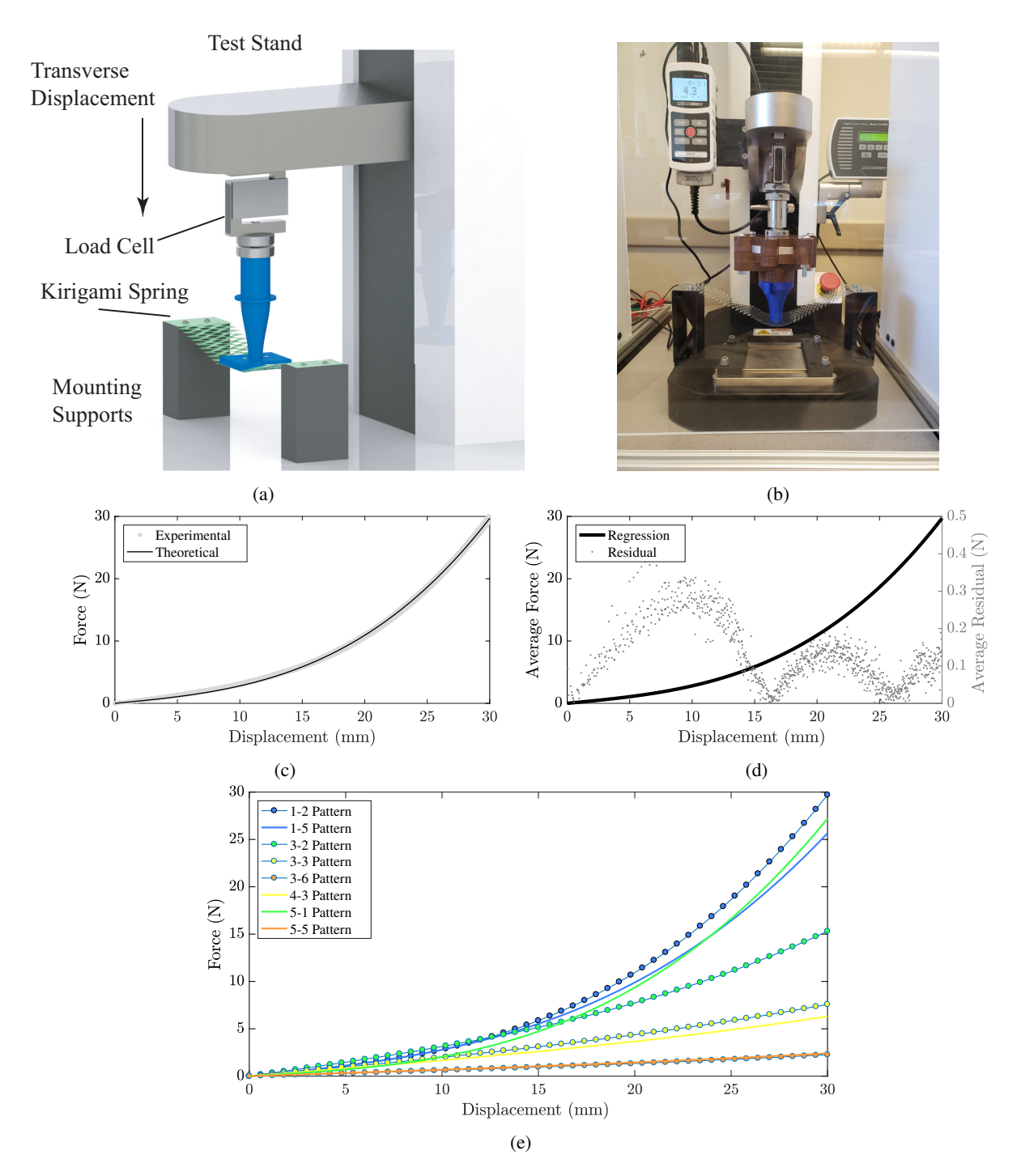


**FIGURE 3**: Quasi-static characterization of kirigami springs: (a) Schematic and (b) image of force vs. displacement test. (c) Theoretical and experimental force versus displacement for 1-2 pattern. (d) Theoretical fit and residual for force versus displacement for 1-2 pattern. (e) Force versus displacement relationship for all patterns considered.

## 6 Dynamic Testing

In order to refine the stiffness parameters and to determine damping of the kirigami springs an impact hammer was used to

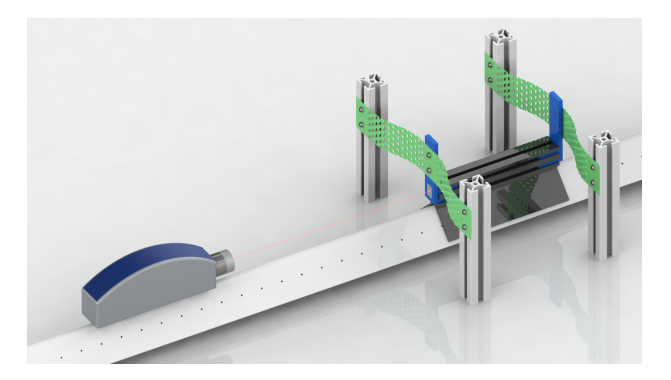


**FIGURE 4**: Schematic of the dynamic test apparatus. The two kirigami springs (in green) are attached to the sliding mass through the 3D printed support (blue) and to the pre-stretch system (vertical bar). The velocity of the system was measured with the Polytec OFV 501/Fiber Interferometer Laser vibrometer; the Data Physics Abaqus DP 901-6C DSP acquisition system, not depicted in figure, complete the experimental set-up.

initiate a transient response of spring attached to a mass, creating a single degree of freedom oscillator. Figure 4 shows the experimental setup used to determine the model parameters. The system is composed of two pre-streched nonlinear kirigami springs connected to a mass through 3D printed supports. The mass is free to oscillate on the friction-less track with a triangular profile, with outlet holes that allows air to escape resulting in low friction movement of the mass as it glides along the track. The inlet pressure for the air-truck is 0.5 psi. The total mass of the cart and the 3D printed supports is 118.4 g while the springs' mass is assumed to be negligible. The velocity of the system is acquired using the Polytec OFV 501/Fiber Interferometer laser vibrometer and the Data Physics Abaqus DP 901-6C DSP is used for data acquisition. The velocity response is measured for 25 seconds.

#### 7 PARAMETER ESTIMATION

This section details both the parameter estimation using both the quasi-static and transient response test. The primary parameters of the spring are it stiffness components as well as the energy loss parameters associated with plastic.

## 7.1 Characterizing the Static Stiffness

Before attempting to characterize the stiffness of each spring, the form of the force displacement relationship must first be determined. Using the observations from Eqn. (3), the geometric nonlinearity is assumed elastic and the resistive force exerted by the spring is assumed to be a cubic polynomial of the

form

$$F(x) = k_1 x + k_3 x^3, (4)$$

where  $k_1$  is linear stiffness and  $k_3$  is the cubic stiffness. The test data for each spring was fit to this form using iteratively reweighted least-squares (IRLS) [12] in Matlab and the coefficients  $k_1$  and  $k_3$ . Note the loss mechanism is not captured in these test and the next section presents a mechanism to quantify damping.

## 7.2 Dynamic Model

The equation of motion a single degree of freedom oscillator with two kirigami springs in series and floating on a frictionless track can be written as

$$\ddot{x} + c_1 \dot{x} + c_2 \dot{x} |\dot{x}| + c_3 \dot{x}^3 + \bar{k}_1 x + \bar{k}_2 x^2 + \bar{k}_3 x^3 = 0,$$
 (5)

where x is the displacement of the mass  $\bar{k}_1$ , and  $\bar{k}_3$  are the linear and cubic stiffness whose initial estimates are provided from the quasi-static test. The  $k_2$  is to account for asymmetries due to misalignment of the springs. Furthermore, the damping has linear and cubic coefficients of  $c_1$  and  $c_3$ , respectively. The quadratic damping coefficient  $c_2$  is again due to misalignment. In this case, the mass is tilted slightly while oscillating on the track, leading to some air resistance. It is worth noting that the linear and cubic stiffness terms were determined using the experimental tension tests described previously. Additionally, it should be also noted that the  $\bar{k}_1$  and  $\bar{k}_3$  as the appear in the Eqn. (6) are the equivalent spring stiffness of two nonlinear springs in series obtained as in Radomirovic et al. [13] based on the values of stiffness ( $k_1$  and  $k_3$ ) from the fit in Eqn.(4). Finally, it should be noted that the equations of motion are in the form of Helmholtz-Duffing oscillator with nonlinear damping [14].

Examining the system, the stiffness and damping coefficients are unknown. This model simplifies the energy loss mechanism to a nonlinear viscous term, in which the damping mechanism is a function of the velocity that opposes relative motion between the mass and the track. To facilitate an analytical solution, the equation of motion is cast in non-dimensional form using respectively a characteristic length scale of the system  $(L_c)$ , which we assumed to be the pre-stretch of the springs, and a time scale  $\tau = \omega_n t$ . Using these transformations, the non-dimensional equations of motion can be written as

$$\ddot{\chi} + \hat{c}_1 \dot{\chi} + \hat{c}_2 \dot{\chi} |\dot{\chi}| + \hat{c}_3 \dot{\chi}^3 + \chi + \hat{k}_2 \chi^2 + \hat{k}_3 \chi^3 = 0,$$
 (6)

where the non-dimensional terms are defined as

$$\chi = \frac{x}{L_c}, \quad \tau = \omega_n t, \quad \Omega = \frac{\omega}{\omega_n}, \quad \hat{c}_1 = \frac{c_1}{m\omega_n},$$

$$\hat{c}_2 = \frac{c_2 L_c}{m}, \quad \hat{c}_3 = \frac{c_3 \omega_n L_c^2}{m}, \quad \hat{k}_2 = \frac{\bar{k}_2 L_c}{\bar{k}_1}, \quad \hat{k}_3 = \frac{\bar{k}_3 L_c^2}{\bar{k}_1}.$$

In the following, uniformly valid solutions for the equation in (6) are obtained using the Method of Multiple Scales for the motion in free vibration.

## 7.3 Method of Multiples Scales

It is convenient to reorganize the equation of motion by introducing a book keeping parameter  $\varepsilon$  and collecting terms with the same order. The equation of motion can be written as follows

$$\ddot{\chi} + \chi + \varepsilon \hat{k}_2 \chi^2 + \varepsilon^2 \left( \hat{k}_3 \chi^3 + \hat{c}_1 \dot{\chi} + \hat{c}_2 \dot{\chi} |\dot{\chi}| + \hat{c}_3 \dot{\chi}^3 \right) = 0. \tag{7}$$

Note that the damping coefficients and the cubic stiffness are scaled at order  $\varepsilon^2$  and the quadratic stiffness term is scaled on the order of  $\varepsilon$ . This implies that the following inequality must hold  $\hat{k}_3 < \hat{k}_2 < \hat{k}_1$  for the asymptotic solution presented below to be valid.

The initial conditions can be written in their non-dimensional form as  $\chi(0) = x(0)/L_c$  and  $\dot{\chi}(0) = \dot{x}(0)/(L_c\omega_n)$ . The time dependence is expanded into multiple scales  $T_n = \varepsilon^n \tau$ , and the time derivatives can be written as

$$\frac{\partial}{\partial t} = D_0 + \varepsilon D_1 + \varepsilon^2 D_2 + \mathcal{O}(\varepsilon^3), \tag{8a}$$

$$\frac{\partial^2}{\partial t^2} = D_0^2 + 2\varepsilon D_0 D_1 + \varepsilon^2 \left( D_1^2 + 2D_0 D_2 \right) + \mathcal{O}(\varepsilon^3), \tag{8b}$$

where  $D_n = \partial/\partial T_n$ . Furthermore, the time-dependent non-dimensional displacement  $\chi$  can be expressed as

$$\chi(t;\varepsilon) = \sum_{i=0}^{2} \varepsilon^{i} \chi_{i}(T_{0}, T_{1}, T_{2}) + \mathscr{O}(\varepsilon^{3}). \tag{9}$$

Substituting Eqns.(8) and (9) in the Eqn.(7) and gathering terms with the same power of  $\varepsilon$  yields

$$\mathcal{O}(\varepsilon^0): D_0^2 \chi_0 + \chi_0 = 0, \tag{10a}$$

$$\mathscr{O}(\varepsilon^1): D_0^2 \chi_1 + \chi_1 = -2D_0 D_1 \chi_0 - \hat{k}_2 \chi_0^2, \tag{10b}$$

$$\mathcal{O}(\varepsilon^{2}): D_{0}^{2}\chi_{2} + \chi_{2} = -2D_{0}D_{1}\chi_{1} - D_{1}^{2}\chi_{0} - 2D_{0}D_{2}\chi_{0} - 2\hat{k}_{2}\chi_{0}\chi_{1} - \hat{k}_{3}\chi_{0}^{3} - \hat{c}_{1}D_{0}\chi_{0} - \hat{c}_{3}(D_{0}\chi_{0})^{3} - \hat{c}_{2}\left(g_{1}\exp(iT_{0})dT_{0} + \sum_{\substack{n=0\\n\neq 1}}^{\infty}g_{n}\exp(inT_{0})\right),$$
(10c)

where g's are the Fourier's coefficients used to approximate the function  $\dot{x}|\dot{x}|$ ,  $g_n=g_n(A,\bar{A})$ .

Solutions to the  $\mathscr{O}(\varepsilon^0)$  expansion in Eqn. (10a) can be written as

$$\chi_0 = A(T_1, T_2) \exp(iT_0) + \bar{A}(T_1, T_2) \exp(-iT_0),$$
 (11)

where  $\bar{A}$  is the complex conjugate of A. Substituting into Eqn. (10b) yields

$$D_0^2 \chi_1 + \chi_1 = -2iD_1 A \exp(iT_0) - \hat{k}_2 \left( A^2 \exp(2iT_0) + A\bar{A} \right) + cc,$$
(12)

where cc denotes complex conjugate. To derive uniformly valid expansion, we must eliminate secular terms from the Eqn. (12) hence,  $D_1A = 0$ ; therefore,  $A = A(T_2)$ . The solution Eqn. (12) can be written as

$$\chi_1 = \hat{k}_2 \left( \frac{A^2}{3} \exp(2iT_0) - A\bar{A} \right) + cc.$$
(13)

In view of the Eqns. (11) and (13), the  $\mathcal{O}(\epsilon^2)$  expansion in (10c) writes

$$D_{0}^{2}\chi_{2} + \chi_{2} = \left(2iD_{2}A + i\hat{c}_{1}A + \frac{i\hat{c}_{2}A^{2}}{2\pi} \int_{0}^{2\pi} \sin^{2}(\phi) |\sin(\phi)| d\phi + 3i\hat{c}_{3}A^{2}\bar{A} + 3k_{3}A^{2}\bar{A} + \frac{10}{3}\hat{k}_{2}^{2}A^{2}\bar{A}\right) \exp(iT_{0}) - \left(2\hat{k}_{2}^{2}A^{2} \left(\frac{A}{3} + 2\bar{A}\right) - \hat{k}_{3}A^{3} - i\hat{c}_{1}A^{3} - i\hat{c}_{3}A^{3}\right) \exp(3iT_{0}) - \hat{c}_{2}\sum_{\substack{n=0\\n\neq 1}}^{\infty} g_{n} \exp(inT_{0}).$$

$$(14)$$

Secular terms can be eliminated from the expression of  $\chi_2$  if

$$i\left(2D_{2}A + \hat{c}_{1}A + \frac{\hat{c}_{2}A^{2}}{2\pi} \int_{0}^{2\pi} \sin^{2}(\phi) |\sin(\phi)| d\phi + 3\hat{c}_{3}A^{2}\bar{A}\right) + 3k_{3}A^{2}\bar{A} + \frac{10}{3}\hat{k}_{2}^{2}A^{2}\bar{A} = 0,$$
(15)

where  $\phi = T_0 + \beta$ . It is then convenient to express A in polar form, i.e.

$$A = \frac{1}{2}a\exp\left(i\beta\right),\tag{16}$$

where a and  $\beta$  are real functions of the time scale  $T_2$ . Following that, by substituting Eqn.(16) into Eqn.(15) and separating the real and imaginary parts, the following set of equations is obtained.

$$\dot{a} = -\frac{\hat{c}_1}{2}a - \frac{4\hat{c}_2}{3\pi}a^2 - \frac{3\hat{c}_3}{8}a^3$$
, and (17a)

$$a\dot{\beta} = \frac{10\hat{k}_2^2 - 9\hat{k}_3}{24}a^3. \tag{17b}$$

Finally,  $a_0$  and  $\beta_0$  are evaluated imposing the initial conditions as follows

$$a_0 \cos(\beta_0) = 0$$
 and  $a_0 \sin(\beta_0) = -\dot{\chi}(0)$ , (18)

which yields

$$a_0 = -\dot{\chi}(0)$$
, and  $\beta_0 = \frac{\pi}{2} + 2m\pi$ , where  $m \in \mathbb{Z}$ . (19)

The modulation equations (17) were solved via numerical integration. Once the numerical solutions for the equations in (17) is obtained, the zeroth-order time response can be reconstituted as

$$\chi = a(\tau)\cos(\tau + \beta(\tau)). \tag{20}$$

A numerical optimization is used to fit the experimental time responses to that obtained via numerical integration using the Dormand-Prince Runge-Kutta integration scheme [15]. The objective optimization was to determine the unknown parameters, i.e. the quadratic stiffness term and the damping terms which minimize a modified least square functional. Each recorded time history is truncated. Notably, we used the first 10 seconds to calculate the damping coefficients and the quadratic stiffness. The parameters obtained via the optimization were then used to compare the experimental and numerical velocities over the full 25 seconds window. An example of the results obtained using this procedure is presented in Figure 5. Further details concerning the optimization are reported in the Appendix 9.

The time traces match closely for the first ten seconds and then exhibit a distinct phase shift, indicating that the modulation equations governing phase do not accurately represent the response; this is most likely due to an incomplete nonlinear damping model. However, the amplitudes closely match throughout the time interval.

## 8 Results and Discussion

This section discusses the results of the quasi-static fit and the dynamic testing of parameters. The discussion begins with the quasi-static results.

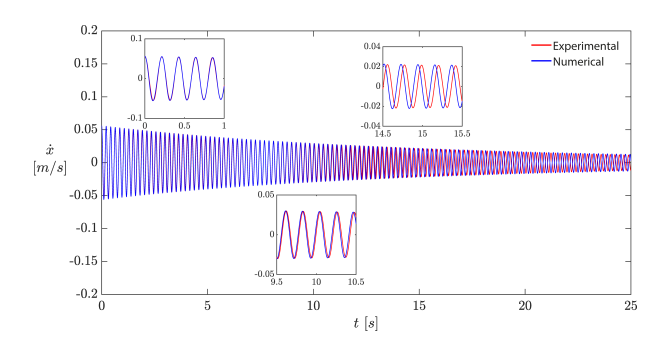


**FIGURE 5**: Comparison of the experimental and numerical (Dormand-Prince Runge-Kutta) velocity with respect to time for spring with pattern 5-5. The two curves overlap for the entire time window used for the optimization ( $\Delta t = 10$  seconds) then the two signal drift yet having the same amplitude.

Figure 3 shows sample curve fits for the 1-2 pattern. In particular Fig. 3 (c) shows the curve fit for the average loading and unloading curves, and Fig. 3 (d) shows the curve fit and residuals between the curve fit and the loading and unloading data, note that they are an order of magnitude lower than curve fit values. Finally, Fig. 3 (e) shows the curve fits fo the force versus displacement for all patterns Table 1 shows the average linear and cubic stiffness and the standard deviation in their values obtained from the quasi-static test. Notably the measurements are quite similar across the 5 samples for each pattern. In general, patterns with larger cut densities, i.e., 5-5 and 3-6, are more compliant that other patterns. Furthermore there is an order of magnitude difference in linear stiffness between the most and least compliant sample.

For all the systems analyzed, the optimum values for the quadratic spring term and the damping coefficients are reported in Table 2. For completeness we report in Table 2 also the non-dimensional cubic stiffness; by virtue of the non-dimensionalisation, the non-dimensional linear stiffness  $\hat{k}_1 = 1$  for all the system considered and thus is not included in the table. A cursory inspection of the quadratic stiffness terms for the various systems unveils that they are inversely proportional to the  $k_3$ . The quadratic stiffness term's random nature and its limited variability compared  $\hat{k}_1$  and  $\hat{k}_3$  allow us to conclude that the quadratic term is unrelated to the kirigami pattern and is mainly due to misalignment of the two springs as speculated above.

In Figure 6 we compare the amplitude of vibrations calculated with the method of multiple scales against the velocity measured experimentally. Although we used only the first order approximation, i.e  $\chi_0$ , and regardless of the pattern considered, we found that the predicted and measured amplitude are in good agreement.

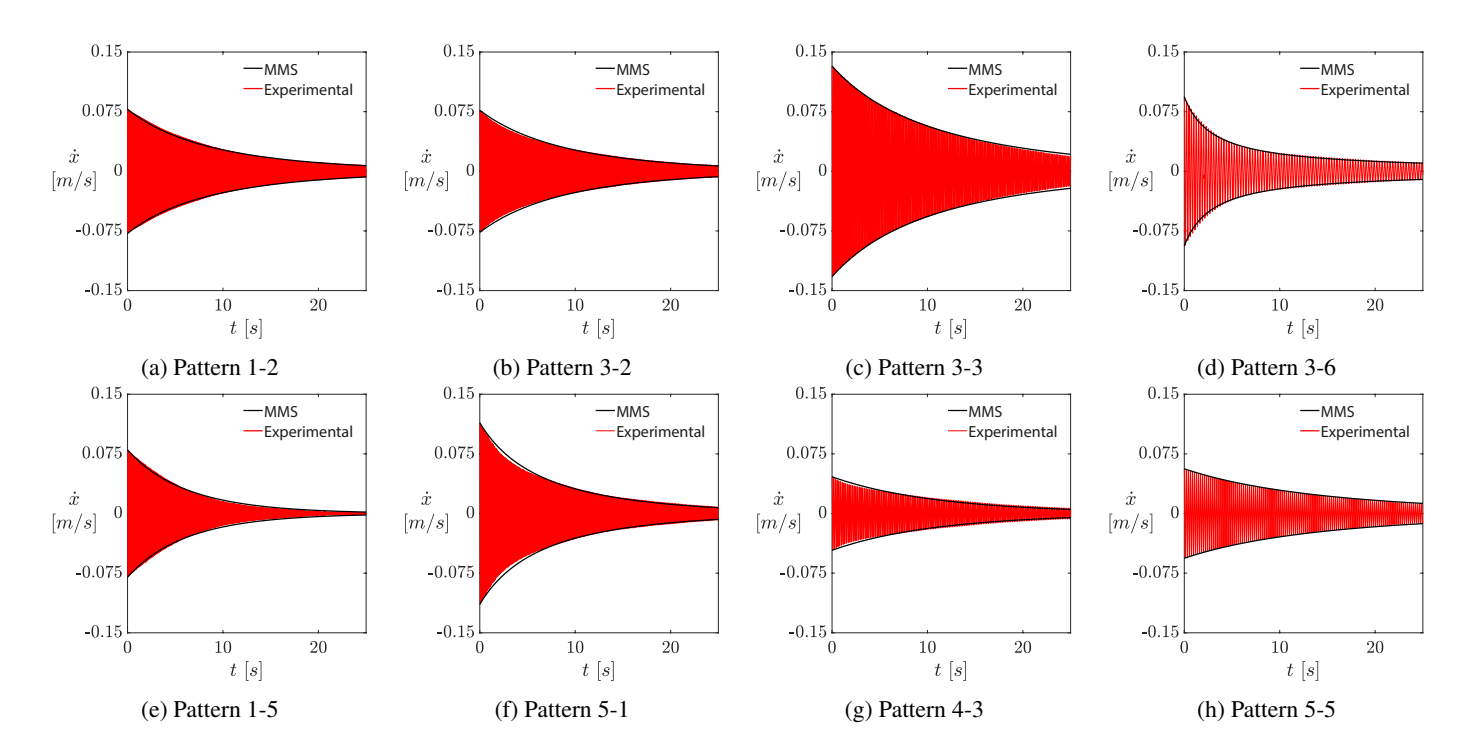


**FIGURE 6**: Comparison of the experimental time responses against the amplitude of vibrations as predicted using the Method of Multiple Scales for springs. Experimental time responses are in red, amplitude of vibrations are in black.

Pattern	k <sub>1</sub> (N/mm)		k <sub>3</sub> (N/mm <sup>3</sup> )	
	Average	Standard	Average	Standard
		Deviation		Deviation
1-2	0.1912	0.007978	8.8781E-4	1.3710E-5
1-5	0.2061	0.009597	7.2126E-4	1.4630E-5
3-2	0.2877	0.008847	2.4723E-4	3.5371E-5
5-1	0.1172	0.004096	8.7702E-4	1.1205E-5
3-3	0.1913	0.004917	6.8183E-5	6.8874E-6
4-3	0.1620	0.010473	5.3534E-5	4.9023E-6
3-6	0.0597	0.004949	1.7500E-5	7.6658E-7
5-5	0.0663	0.002295	1.5588E-5	1.4443E-6

**TABLE 1**: Average and standard deviation of experimental linear and cubic stiffness for each spring pattern.

#### 9 Conclusions

Kirigami, the ancient Japanese art of paper cutting, has the potential to enable the development of structures with tunable

**TABLE 2:** Non-dimensional parameters for the various systems considered in the present study. The results pertain the BC series. The non-dimensional linear spring stiffness is  $\hat{k}_1 = 1$  for all the system considered.

Pattern	$\hat{k}_2$	$\hat{k}_3$	$\hat{c}_1$	$\hat{c}_2$	$\hat{c}_3$
1-2	3.4609E-1	3.8998E-2	2.7999E-3	3.5159E-3	6.1803E-4
1-5	3.8948E-2	4.2529E-2	5.6999E-3	1.5304E-3	1.1713E-3
3-2	4.3608E-2	1.4387E-2	3.5599E-3	2.8928E-3	3.3471E-4
5-1	4.1282E-2	5.4289E-2	3.3999E-3	5.0544E-3	.7514E-4
3-3	2.2639E-1	7.1657E-3	2.5999E-3	2.4246E-3	2.3515E-4
4-3	2.0242E-1	6.7939E-3	4.8043E-3	1.2186E-3	7.2505E-5
3-6	3.3564E-1	3.8560E-3	1.9993E-4	2.3226E-2	1.7980E-3
5-5	1.8475E-1	2.7833E-3	3.2011E-3	2.9852E-3	2.3884E-4

elastic properties. The purpose of this manuscript is to characterize plastic kirigami springs for use in vibration applications. The spring's elastic and damping properties are determined in two steps. Elastic and viscous behavior are assumed to be decoupled. The first step employs quasi-static analysis to quantify the stiffness associated with the geometric nonlinearity that occurs as the spring deforms. The springs have a cubic force versus dis-

placement curve. The damping properties of a single degree of freedom oscillator with kirigami springs are determined using the transient response. The modulation equations are derived using the Multiple Scale Method. The modulation equations are solved numerically and used to approximate the transient response to a first order level. The damping and stiffness parameters due to asymmetries are determined by matching semi-analytical and experimental results using an optimization algorithm. This study is a first step toward incorporating kirigami-based structures into vibration applications.

#### **ACKNOWLEDGMENT**

The authors would like to acknowledge the financial support provided by NSF CAREER Award: CMMI 2145803 and the Purdue Research Foundation (PRF)

## Appendix A: OPTIMIZATION

The optimization was implemented in Matlab's by means of the *fmincon* function and using the interior-point algorithm. The optimization variables were the quadratic stiffness term and the damping coefficients. Denoting with  $\dot{\chi}$  the velocity of the system governed by the Eqn.(6) and with TH the non-dimensional experimental time history, the optimization problem write

$$\min_{C^{i}} \sum_{t \in [0,10]} \left( \dot{\chi} - TH \right)^{2} \max \left( |\dot{\chi} - TH| \right),$$
**subject to:**  $\hat{k}_{3} \leq \hat{k}_{2} \leq \hat{k}_{1},$ 

$$0 \leq \hat{c}_{1} \leq \eta \ \hat{c}_{cr},$$

$$0 \leq \hat{c}_{2} \leq \eta \ \hat{c}_{cr},$$

$$0 \leq \hat{c}_{3} \leq \eta \ \hat{c}_{cr}.$$
(21)

where  $C = \{\hat{c}_1, \hat{c}_2, \hat{c}_3, \hat{c}_2\}$  and  $\eta \ll 1$ . For each SDOF oscillator, we minimized the residual between the experimental time history and the numerical solutions of the SDOF. For the optimization we considered only the first 10 seconds of the time histories.

#### **REFERENCES**

- [1] Bruton, Jared T, Nelson, Todd G, Zimmerman, Trent K, Fernelius, Janette D, Magleby, Spencer P and Howell, Larry L. "Packing and deploying Soft Origami to and from cylindrical volumes with application to automotive airbags." *Royal Society open science* Vol. 3 No. 9: p. 160429.
- [2] Sargent, Brandon, Butler, Jared, Seymour, Kendall, Bailey, David, Jensen, Brian, Magleby, Spencer and Howell, Larry.

- "An origami-based medical support system to mitigate flexible shaft buckling." *Journal of Mechanisms and Robotics* Vol. 12 No. 4.
- [3] Faber, Jakob A, Arrieta, Andres F and Studart, André R. "Bioinspired spring origami." *Science* Vol. 359 No. 6382 (2018): pp. 1386–1391.
- [4] Yang, Yi, Vella, Katherine and Holmes, Douglas P. "Grasping with kirigami shells." *Science Robotics* Vol. 6 No. 54 (2021): p. eabd6426.
- [5] Jin, Lishuai, Forte, Antonio Elia, Deng, Bolei, Rafsanjani, Ahmad and Bertoldi, Katia. "Kirigami-inspired inflatables with programmable shapes." *Advanced Materials* Vol. 32 No. 33 (2020): p. 2001863.
- [6] Rafsanjani, Ahmad, Zhang, Yuerou, Liu, Bangyuan, Rubinstein, Shmuel M and Bertoldi, Katia. "Kirigami skins make a simple soft actuator crawl." *Science Robotics* Vol. 3 No. 15 (2018): p. eaar7555.
- [7] Rafsanjani, Ahmad, Jin, Lishuai, Deng, Bolei and Bertoldi, Katia. "Propagation of pop ups in kirigami shells." *Proceedings of the National Academy of Sciences* Vol. 116 No. 17 (2019): pp. 8200–8205.
- [8] Soleimani, H., Goudarzi, T. and Aghdam, M.M. "Advanced structural modeling of a fold in Origami/Kirigami inspired structures." *Thin-Walled Structures* Vol. 161 (2021): p. 107406.
- [9] Zhu, R, Yasuda, H, Huang, GL and Yang, JK. "Kirigami-based elastic metamaterials with anisotropic mass density for subwavelength flexural wave control." *Scientific reports* Vol. 8 No. 1 (2018): pp. 1–11.
- [10] Gandla, Srinivas, Song, Jaewoo, Shin, Jonghwan, Baek, Seungho, Lee, Minwoo, Khan, Danial, Lee, Kang-Yoon, Kim, Jung Ho and Kim, Sunkook. "Mechanically Stable Kirigami Deformable Resonant Circuits for Wireless Vibration and Pressure Sensor Applications." ACS Applied Materials & Interfaces Vol. 13 No. 45 (2021): pp. 54162– 54169
- [11] Yang, Yi, Dias, Marcelo A and Holmes, Douglas P. "Multistable kirigami for tunable architected materials." *Physical Review Materials* Vol. 2 No. 11 (2018): p. 110601.
- [12] Holland, Paul W. and Welsch, Roy E. "Robust regression using iteratively reweighted least-squares." *Communications in Statistics Theory and Methods* Vol. 6 No. 9 (1977): pp. 813–827.
- [13] Radomirovic, Dragi and Kovacic, Ivana. "An equivalent spring for nonlinear springs in series." *European Journal of Physics* Vol. 36 No. 5 (2015): p. 055004.
- [14] Kovacic, Ivana and Gatti, Gianluca. "Helmholtz, duffing and helmholtz-duffing oscillators: exact steady-state solutions." *IUTAM Symposium on Exploiting Nonlinear Dynamics for Engineering Systems*: pp. 167–177. 2018. Springer.
- [15] Dormand, John R and Prince, Peter J. "A family of embed-

ded Runge-Kutta formulae." *Journal of computational and applied mathematics* Vol. 6 No. 1 (1980): pp. 19–26.